

PMU-Based Artificial Intelligence Techniques for Islanding Detection

SEBA ALGHARAIBEH¹, MOHAMMAD ALMOMANI¹, TAMADHER ALMOMANI², MALIK ALKASASBEH¹, ALI ALDMOUR¹

¹Electrical Engineering Department, Mutah University, Karak, JORDAN

²Department of electrical engineering, Al-Balqa Applied University, As Salt, JORDAN

Abstract- This paper presents an islanding detection method (IdM) based on phasor measuring unit (PMU) technology. The PMUs are used to measure the synchronized data and collect it in real-time. Three PMUs are located in this work to obtain full observability: at distributed generator (DG) side, load location, and point of common coupling (PCC). The measured signals are directly fed to the classifier to identify the islanding events. This algorithm shows that the proposed method can detect the islanding with 100% detection accuracy and zero non-detection zone (NDZ). Both DG types are tested in this paper: inverter-based DG and rotating machine-based DG. The detection time of the remote method is five cycles for the inverter-based test system and seven cycles for the rotating machine test system.

Key-Words: Artificial Neural Network (ANN), Decision Tree (DT), Islanding Detection Method (IdM), K-nearest Neighbor Algorithm (KNN), Support Vector Machine (SVM), rotating machine DG, inverter-based DG.

1 Introduction

The rapid increase in electrical demand with the problem of fuel consumption creates a serious need for renewable energy resources. This green energy reduces the impacts of using fuel to generate electricity by using sunlight [1], wind energy, hydropower, tidal energy, geothermal energy, and other renewable energies. These distribution generators (DG) are connected in a micro-grid (MG) at the distribution level. Any MG can be operated in two conditions: islanding and non-islanding. The islanding operation of the micro-grid can be clearly defined when the PCC is identified. The PCC is an electrical connection point depending on the distribution network operators and the MG's owner (or operator). The MG may be islanded for different cases such as faults inside the MG, overload, maintenance purposes, failure in the DG system ... In islanding mode, the frequency and voltage are the most critical issues to be considered in the controller; whereas, the power control in MG is a vital issue in a non-islanding mode. In some cases, the MG does not work in islanding mode, so the DGs are gotten down if the MG senses an islanding event. Therefore, to convert the control mode from islanding to non-islanding mode or turn off the DGs, an accurate islanding-detection method (IdM) is needed.

IdMs are generally categorized as local and remote methods. Regional techniques are categorized as hard computing and soft computing method; furthermore, hard computing methods are classified into passive, active, and hybrid. On the

other hand, soft computing methods can be classified based on an intelligence-based algorithm and signal processing algorithms. Moreover, remote IdMs can be categorized into power line carrier communication (PLC), supervisory control and data acquisition (SCADA), trip transfer method (TTM), and wide-area measurement system (WAMS).

A new artificial neural network-based method for islanding detection of distributed generators is presented in [2]. The authors use the voltage at the PCC to train four layers of ANN with 8, 4, 2, and 1 perceptron per layer, respectively. The voltages are collected with two sample rates: 64 sample/cycle and 128 sample/cycle; then, they are used as input to the ANN. The data window is a complete cycle, and the algorithm acquaints the data cycle-by-cycle. The proposed algorithm can detect the islanding within nine cycles for the island and 18 cycles for non-island events. The algorithm is tested for a 0.1-1 Pu power mismatch. The NDZ is less than 0.25 Pu in the 64 sample/cycle system and less than 0.15 Pu in the 128 sample/cycle system. The NDZ in this algorithm depends on the detection time, where the accuracy of this algorithm reaches 99.88 %, 94.71%, and 92.91% for detection time of 2 sec, 1 sec, and 0.5 sec, respectively.

An islanding detection method using a ridgelet probabilistic neural network is presented in [3]. This paper presents a comparison between the ridge-let probabilistic neural network and PNN. The voltage at the PCC is measured, and six features are extracted from the measured three-phase voltage: mean, maximum, minimum, standard deviation,

energy, and entropy. Inverter-based DG is used to verify the accuracy of this algorithm. The accuracy of this algorithm is 100%, with a small NDZ ($< 3\%$) at quality factor =1. Time detection is 0.188sec.

Islanding detection using SVM is presented by [4]. Researchers propose an IdM for single-phase inverter-based DG. The features are extracted for the voltage and current signal at the PCC using the autoregression modelling technique. Then, the SVM is learned under different scenarios of islanding and non-islanding. This method can detect islanding cases within 50 ms. The NDZ in this method is zero. Other applications of WAMS that covered various power system aspects are presented in [5-8].

2 Systems Understudy

In this study, two test systems are presented to cover all DGs scenarios. PV-test system is modelled as an example on inverter-based DG, and doubly fed induction generator (DFIG) test system is modelled as an example on rotating machine-based DG system.

2.1 DFIG-based Test System

The single line diagram of the DFIG-based DG test system is shown in Figure 1. This system is modelled by MATLAB 2020a/Simulink platform.

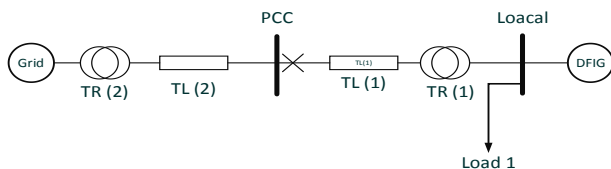


Fig. 1: DFIG-Based DG test system

This test system consists of one DFIG connected to a load at 515 V level, a step-up distribution transformer 515V/25 kV, and a step-up power transformer to change the medium voltage (25 kV) to high voltage connect with the primary grid (120 kV).

The detailed parameters of the DFIG are attached in Table A-1 in the appendix. The DFIG in this test system consists of 6 turbines. In Table A-1, generator parameters, turbine parameters, converter parameters, controller parameters, and drive train parameters are presented per turbine. The total rated power of the DFIG is (1.5MW \times 6 turbines). Load 1 is changed to achieve different power mismatches regarding the standards [2]. Load 1 is modelled as a constant impedance load. Load quality factors are selected to be 1 in this research.

The MG in this test system is connected to the PCC via a 10 Km transmission line (TL1). The

system consists of a low-voltage load (L1) at the DG-connected point. The medium-voltage station (PCC) is connected to a robust grid (infinite bus) via a 20 Km transmission line (TL2). Table A-2 in the appendix shows the system parameters' values: transformers, lines, and the primary grid.

2.2 PV-Based Test System

The single line diagram of the PV-Based DG test system is shown in Figure 2. Like the previous test system, the MATLAB 2020a/ Simulink platform is used to model this system.

In this system, the DG is connected to the 250 V side, then the power is transformed to 25KV level at the load side, and the grid is connected at 120 kV. The system operates under 60 Hz, and the nominal power of the DG is 250 KW. The DG is connected to the PCC via a step-up transformer (250V/25KV), and the local load (Load 1) is connected at the PCC in the medium voltage level. This load is changed to achieve different real and reactive power mismatches.

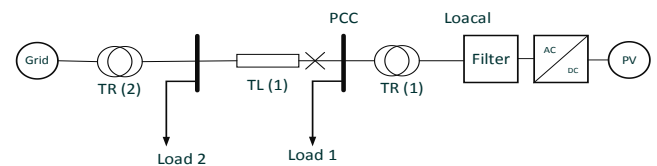


Fig. 2: PV-Based DG test system

PV parameters, converter parameters, and filter parameters are attached in Table A-3 in the appendix. System parameters (transformer 1 and 2, transmission line, load, grid) are shown in Table A-4 in the appendix. The maximum power point tracking controller in this system is based on perturbing and observation (P&O). A 3-bridge IGBT converter is used to convert the DC-generated power to 60 HZ AC power.

These two test systems are used to validate the proposed IdM in the following sections. The simulations are run several times under different power mismatches for three events: increasing local load, decreasing local load, and islanding event. The islanding scenarios are achieved by opening the circuit breaker at the PCC for both systems.

3 Proposed Algorithm

This paper has three PMUs installed at the DG connected point, load connection, and PCC. For a huge system, optimal PMUs placements should be identified firstly [9]. From each PMU, the synchronized voltage (magnitude and angle), frequency, ROCOV, and ROCOF are measured. The sample rate of the PMU is 1 sample/cycle refer to

std. IEEE C118.2004. So, the number of the features here are 15 (five at PCC, five at DG point, and five at the load). Three types of events are covered: switch on (inductive/ capacitive/ resistance) load, switch of (inductive/ capacitive/ resistance) load, and islanding events. The number of events is shown in Table 1. These events cover real power imbalance from -33% to 33% with step size 6% for non-islanding events and 3% for islanding events, and imbalance reactive power from -22% to 22% with step size 4%.

Table 1. Events and islanding

Event	Inductive	Capacitive	Resistance
Switch on load	55	55	11
Switch off load	55	55	11
Islanding	242		
Total	484		

From each event, one cycle before the event and ten cycles after the event are collected. All features are computed within this period. The sampling technique is based on cycles; for the one-cycle sampling, the features are calculated for each cycle and represented as a sample; so, the length of the all-feature matrix in one cycle sampling is (484 events \times 11 cycle = 5324) with a width equal to the total number of features (15 features).

The move rate in more than one cycle sampling is just one cycle; for example, in three-cycle sampling, the first sample covers the first three cycles, and the second sample covers the 2nd, 3rd, and 4th cycles, where the third sample covers the cycles between the 3rd and 5th. The islanding event is obtained when the half cycles in a sample become islanding. For example, if the islanding occurs at the end of cycle number 4 and the sampling size is 5 cycles, the first sample, which covers the first five cycles considered a non-islanding event, and the second sample which covers the cycles between the second and the sixth is also regarded as a non-islanding event. However, the samples above the second are considered islanding because the number of islanding cycles is greater than that of non-islanding cycles within their period.

Four classification methods are used to predict the islanding events: support vector machine (SVM), k-nearest neighbours' algorithm (KNN), decision tree algorithm (DT), and artificial neural network as a classifier (ANN).

3.1 Support Vector Machine (SVM)

SVM is a classifier that uses a separating hyperplane to classify data. SVM uses kernel functions to

identify the optimal hyperplane to classify the given data with the minor error for a given labelled dataset, where the input space is projected into a high-dimensional feature space [10].

3.2 k-Nearest Neighbors (KNN)

KNN is a non-parametric Machine Learning algorithm based on the Supervised Learning technique. The KNN algorithm assumes that the new case/data and existing cases are similar, and it places the new case in the closest category to the existing ones. The KNN algorithm saves all available data and classifies a unique data point based on its similarity to the current data. So, the new data can be quickly classified into a well-defined category using the KNN algorithm [11].

3.3 Decision Tree (DT)

DT is a hierarchical model that breaks down a complex decision-making problem into a series of simple decisions. The root node, which contains the initial classification problem, is recursively split into child nodes using a top-down methodology. This splitting continues until the leaf node is reached, i.e., until a classification has been established [12].

3.4 Artificial Neural Network (ANN)

An ANN is a technique for creating a network of neurons that works similarly to a biological neural network. It can recognize patterns and learn from them by using functions that transform data and forward them as activation functions to other neurons in the next layer. The process will be repeated until a neuron in the output layer is activated to identify the specific dataset that needs to be found.

4 Results and Discussions

The Four classification methods are applied to the extracted features (15 Features) for the different samples' sizes. The total events, Table 1, are divided into 80% for the training, 20% for the testing, and 20% for the validation. The results of the four classification methods for both test systems are presented in the following subsections.

4.1 Rotating-Based DG Test System

ROC curves of the different classification methods for the PMU model are presented in Figure 3. ROC curve is plotted between false alarm and detection rate. In IdMs, false alarm means the algorithm detects islanding for non-islanding events, and the detection rate is the percent of the true detection of the islanding events. For Figure 3, the detection rate

reaches 100% in just two classification algorithms: KNN and DT. The detection rate reaches 100% for the sampling greater than or equal to five cycles in KNN and greater than or equal to seven cycles using DT.

From the figure, the false alarms for the one-cycle sampling are about 2% in SVM, 5% in KNN, 6% in DT, and 0.5% in ANN; so, 2%, 5%, 6%, 0.5% of the non-islanding events are falsely detected as islanding in SVM, KNN, DT, and ANN, respectively. On the other hand, the detection rates reach about 70%, 90%, 80%, and 70% at one-cycle sampling for the SVM, KNN, DT, and ANN, respectively. As a conclusion from this figure, the ANN algorithm has the best false alarm value, and KNN has the best detection rate value for the one-cycle sampling.

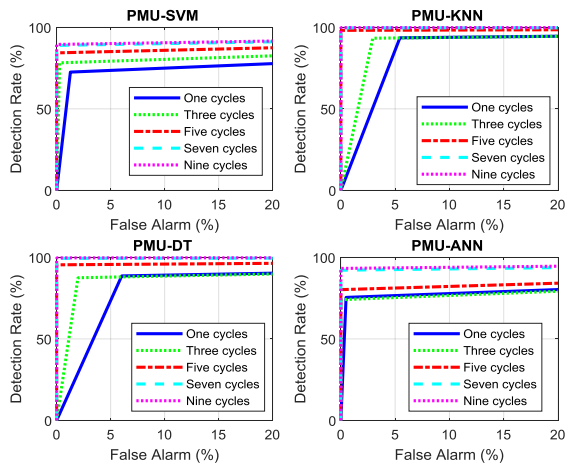


Fig. 3: ROC curves for the DFIG model at different classification methods.

From Figure 3, the effect of the sampling on the false alarm and detection rate can be analyzed as follow:

- The detection rate of the three-cycle sampling is almost equal (actually, it is a little smaller) to the detection rate of the one-cycle in KNN, DT, and ANN, but the false alarms are enhanced in the three-cycle sampling for the four classification algorithms.
- The false alarm reaches about 0 % in five-cycle sampling for the four classification methods.
- The detection rates are enhanced for the seven-cycle sampling in both SNM and ANN, but the detection rate in KNN for the seven-cycle sampling is almost equal to that for the five-cycle sampling.
- The performance of the four methods is matched using seven-cycle and nine-cycle sampling.

In addition to the ROC, the accuracy at different samples is presented in Figure 4. Based on this

figure, the best classification method is KNN. The detection accuracy of the method reaches 100% with zero NDZ for the KNN at sampling equal to 9 cycles; so, the proposed PMU-KNN algorithm can detect the islanding event with zero NDZ within 180 ms.

The accuracy in Figure 4 is defined in equation 1. From the figure, the accuracy of the method is increasing in general with the detection time (sampling); in contrast, the accuracy of the three-cycle sampling is less than that in one-cycle sampling using ANN, that means the effect of decrease the detection rate in Figure 3 is more significant than the enhancement in the false alarm.

$$Accuracy = \left(1 - \frac{\sum |target - output|}{number\ of\ samples} \right) \times 100\% \quad (1)$$

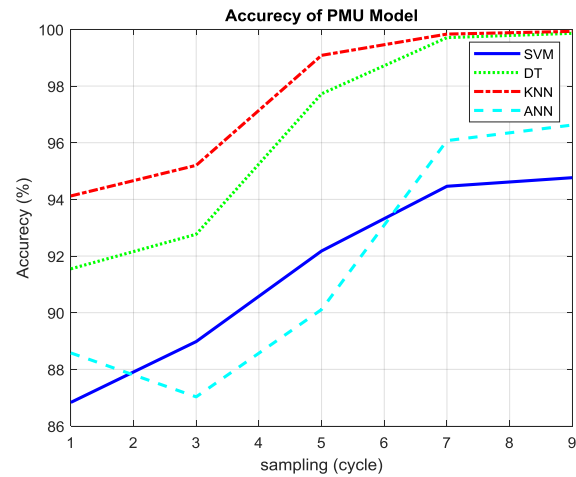


Fig. 4: Accuracy of PMU model for different classification methods.

In Figure 5, true positive (TP), true negative (TN), false positive (FP), and false-negative (FN) for the PMU model using the KNN classification method are presented. The definitions of these indices are:

$$TP = \frac{successfully\ islanding}{number\ of\ islanding} \times 100\% \quad (3.5)$$

$$TN = \frac{successfully\ nonislanding}{number\ of\ nonislanding} \times 100\% \quad (3.6)$$

$$FP = \frac{unsuccessfully\ islanding}{number\ of\ islanding} \times 100\% \quad (3.7)$$

$$FN = \frac{unsuccessfully\ nonislanding}{number\ of\ nonislanding} \times 100\% \quad (3.8)$$

From Figure 5, the FN becomes zero at sample greater than or equal to 5 cycles, and a negligible FP is shown in 7 cycles sampling. For nine sampling cycles, the FP becomes zero, and the TP and TN become 100%.

The NDZ of the KNN-PMU model is shown in Figure 6 to show the performance of the proposed

algorithm to the real/reactive power imbalance. This figure shows the accuracy of the proposed algorithm to the power (real and reactive) mismatches. The accuracy of the outer surface areas is 100%. Then the accuracy decreases between each surface and the next by 5%. From the figure, the NDZs (which is defined here as an area where the accuracy is less than 100%) are shown in the negative real power imbalance at zero reactive power imbalance. The accuracy of the method for any zone is above 90% for five, seven, and eight cycles and above 95% for six cycles. The accuracy of the proposed method is to reach 100% with zero NDZ at sampling equal to nine cycles.

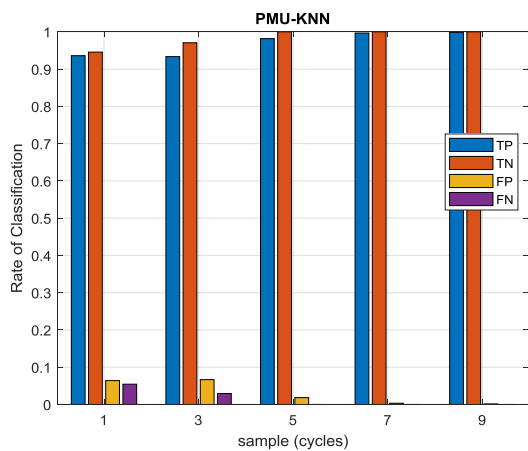


Fig. 5: PMU-KNN Performance, TP, TN, FP, and FN.

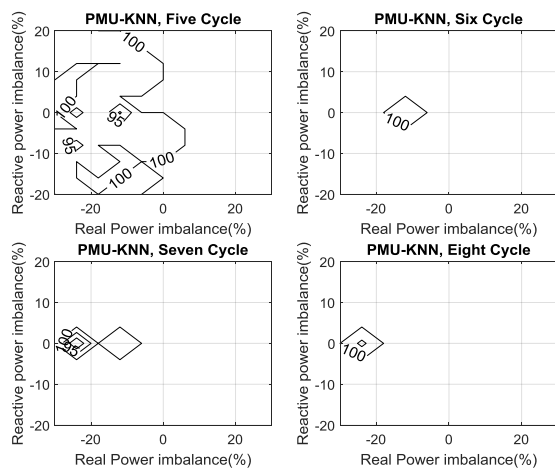


Fig. 6: Accuracy and NDZ of the PMU-KNN

4.2 PMU-AI IdM for Inverter-Based DG

ROC curves of the different classification methods at different sample rates are presented in Figure 7. The detection rate reaches 100% for all methods at a sample rate equal to 7 cycles or above. The best classification algorithm is KNN, where 100% of the detection rate is reached at a sample rate equal to 6 cycles. The four algorithms' performance can be

arranged from the best to the worst based on Figure 7: KNN, DT, SVM, then ANN. The accuracy of all algorithms is reached 100% at a sample rate equal to 7 cycles. The accuracy of the KNN at five cycles sample reaches 99.5%.

Figure 8 shows TP, TN, FP, and FN for the PMU model using the KNN classification method. From the Figure, FN can be neglected at sampling equal to three cycles; the method can detect the islanding events within three cycles, but it needs to at least five cycles to detect the non-islanding events. The accuracy of the KNN method reaches 100% for zero NDZ at sampling equal to 6 cycles or more. The accuracy of the proposed method exceeds 99.9 at a sample rate equal to 5 cycles and above.

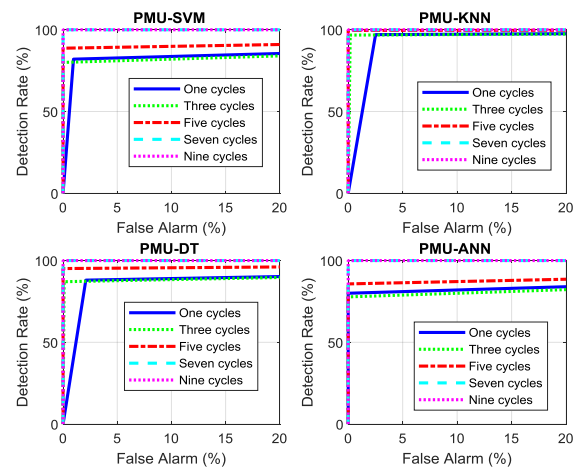


Fig. 7: ROC for PV model at different samplings

The NDZ of the KNN-PMU model is shown in Figure 9. This figure shows the NDZ of the KNN at a sample rate equal to one cycle. The NDZ is limited to the test zone ($\pm 33\%$ real power mismatch and $\pm 22\%$ reactive power mismatch). The accuracy of the detection is greater than 90% for all NDZ. The NDZ is shown in a negative real power mismatch area.

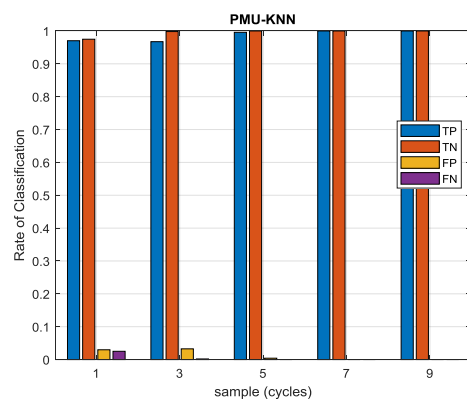


Fig. 8: PMU-KNN Performance, TP, TN, FP, and FN.

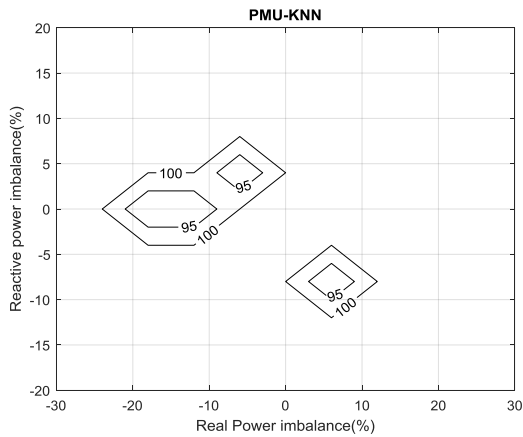


Fig. 9: NDZ of the PMU-KNN

At the end of this section, the results can be summarized in Table 2. This table presents the best accuracy at KNN for inverter-based DG and DT and KNN for rotating machine DG. Table 3 compares the results of the proposed algorithms with the best algorithms from the literature. From the table, the proposed algorithm has the lowest detection time for both DG types.

Table 2. The best accuracy of each method

Test system	Classifier	Accuracy	Cycles
Inverter Based	SVM	100%	7
	DT	100%	7
	KNN	100%	6
	ANN	100 %	7
Rotating Machine	SVM	95%	9
	DT	100%	9
	KNN	100%	9
	ANN	97%	9

Table 3. result Validation

Test System	Ref.	DT (sec)	Accuracy	NDZ
Rotating machine	[2]	2	99.88 %	-
	[13]	0.29	100 %	Zero
	[14]	-	97.77%	Zero
	Proposed	0.18	100%	Zero
Inverter based	[2]	1	94.71 %	-
	[13]	0.37	100 %	Zero
	[14]	-	97.22 %	Zero
	[15]	0.5	97.1 %	<3%
	[16]	0.188	100 %	<3%
	Proposed	0.12	100%	Zero

5 Conclusion

In this paper, the PMU-Based Islanding detection method is proposed. Four artificial intelligence classification algorithms are used here: KNN, ANN, DT, and SVM. The proposed method is tested for

both DG types; inverter-based DG and rotating machine-based DG. The four classification methods are evaluated using ROC curves and detection accuracy. The results show that the proposed algorithm can detect the islanding with 100% accuracy and zero NDZ within 6 and 9 cycles for inverter-based DG and rotating machine-based DG, respectively. The performance of the proposed algorithm concerning the real and reactive power mismatches is presented for the KNN algorithm at different sampling. Finally, the algorithm results are compared with different algorithms from the literature, and the effectiveness of the proposed algorithm is proven.

References

- [1] Almomani, Mohammad, Ali S. Al-Dmour, and Seba Algharaibeh. "Application of Artificial Intelligence Techniques for Modeling and Simulation of Photovoltaic Arrays.", Jordan Journal of Electrical Engineering, 6(4), 2020, PP 296-314.
- [2] Merlin, Victor Luiz, et al. "A new artificial neural network-based method for islanding detection of distributed generators." International Journal of Electrical Power & Energy Systems 75 (2016): 139-151.
- [3] Ahmadipour, Masoud, et al. "Islanding detection method using ridgelet probabilistic neural network in distributed generation." Neurocomputing 329 (2019): 188-209.
- [4] Matic-Cuka, Biljana, and Mladen Kezunovic. "Islanding detection for inverter-based distributed generation using support vector machine method." IEEE Transactions on Smart Grid 5.6 (2014): 2676-2686.
- [5] Odiyat, Abdullah, et al. "Low Frequency Oscillation Analysis for Dynamic Performance of Power Systems." 2021 12th International Renewable Engineering Conference (IREC). IEEE, 2021.
- [6] M. M. Almomani, A. Odiyat, S. F. Al-Gharaibeh and K. Alawasa, "The Impact of Wind Generation on Low Frequency Oscillation in Power Systems," 2021 IEEE PES/IAS PowerAfrica, 2021, pp. 1-5, doi: 10.1109/PowerAfrica52236.2021.9543283.
- [7] Almomani, Mohammad M., and Seba F. Algharaibeh. "Modelling and Testing of a Numerical Pilot Distance Relay for Compensated Transmission Lines." International Journal of Scientific Research and Engineering Development 3.6 (2020): 776-786.

- [8] Al-Momani, Mohammad M., Asmaa SM Hatmi, and Seba F. Al-Gharaibeh. "European Journal of Electrical Engineering." *European Journal of Electrical Engineering* 23.3 (2021): 197-205.
- [9] Al-Odienat, A. I., et al. "Connectivity Matrix Algorithm: A New Optimal Phasor Measurement Unit Placement Algorithm." *IOP Conference Series: Earth and Environmental Science*. Vol. 551. No. 1. IOP Publishing, 2020.
- [10] Vishwanathan, S. V. M., and M. Narasimha Murty. "SSVM: a simple SVM algorithm." *Proceedings of the 2002 International Joint Conference on Neural Networks. IJCNN'02 (Cat. No. 02CH37290)*. Vol. 3. IEEE, 2002.
- [11] Zhang, Min-Ling, and Zhi-Hua Zhou. "ML-KNN: A lazy learning approach to multi-label learning." *Pattern recognition* 40.7 (2007): 2038-2048.
- [12] Rish, Irina. "An empirical study of the naive Bayes classifier." *IJCAI 2001 workshop on empirical methods in artificial intelligence*. Vol. 3. No. 22. 2001.
- [13] Faqhrudin, Omar N., Ehab F. El-Saadany, and Hatem H. Zeineldin. "A universal islanding detection technique for distributed generation using pattern recognition." *IEEE Transactions on Smart Grid* 5.4 (2014): 1985-1992.
- [14] Fayyad, Yara, and Ahmed Osman. "Neuro-wavelet based islanding detection technique." *2010 IEEE Electrical Power & Energy Conference*. IEEE, 2010.
- [15] Kumar, S. Ananda, et al. "A novel islanding detection technique for a resilient photovoltaic-based distributed power generation system using a tunable-q wavelet transform and an artificial neural network." *Energies* 13.16 (2020): 4238.
- [16] Ahmadipour, Masoud, et al. "Islanding detection method using ridgelet probabilistic neural network in distributed generation." *Neurocomputing* 329 (2019): 188-209.

Creative Commons Attribution License 4.0 (Attribution 4.0 International, CC BY 4.0)

This article is published under the terms of the Creative Commons Attribution License 4.0

https://creativecommons.org/licenses/by/4.0/deed.en_US

APPENDIX A

Table A-1. DFIG-DG parameters

Generator parameter /turbine	Value	Converter Parameter/ turbine	Value
Nom. Power (MVA)	1.5/0.9	Grid side current	0.8 Pu
L-L Voltage	575 V	Grid side inductance	0.3 Pu
Frequency	50 Hz	Grid side resistance	0.003 Pu
Stator resistance	0.023 Pu	DC voltage	1150 V
Stator inductance	0.18 Pu	DC bus capacitance	1e-2 F
Rotor resistance	0.016 Pu	Line filter capacitance	120e3
Rotor inductance	0.16 Pu	Controller parameters	Value
Magnetizing inductance	2.9 Pu	DC bus voltage (Kp)	8
Inertia constant	0.685	DC bus voltage (Ki)	400
Pairs of poles	3	Grid side converter (Kp)	0.83
Friction factor	0.01	Grid side converter (Ki)	5
Turbine parameter	Value	Speed regulator (Kp)	3
Output power (MW)	1.5	Speed regulator (Ki)	0.6
Wind speed (m/s)	11	Rotor side converter (Kp)	0.6
		Rotor side converter (Ki)	8
Drive train parameters	Value	Pitch controller (Kp)	3
Wind turbine inertia	4.32 s	Pitch controller (Ki)	30
Shaft spring constant	1.11 torque/rad	Max pitch angle	27
Shaft mutual damping	1.5 Pu	Rate of change of pitch angle	10

Table A-2. DFIG-Based System parameters

TR1 parameters	Value	TL1 Parameters/Km	Value
Vector group	YgD1	Frequency	50 Hz
Nominal power	12 MVA	Pos. seq. resist. (Ohm)	0.1153
Frequency	50 Hz	Zero seq. resist.	1.05e-3
V1/V2	25e3/575	Pos. seq. Inductance	0.413
Win. 1 Resistance	0.001 Pu	Zero seq. Inductance (H)	3.32e-3
Win. 1 Inductance	0.025 Pu	Pos. seq. capacitance(F)	11.33e-9
Win. 2 Resistance	0.001 Pu	Zero seq. capacitance(F)	5-e9
Win. 2 Inductance	0.025 Pu	Line length (Km)	10
Mag. Resistance	500	TL2 Parameters/Km	Value
Mag. Inductance	Inf.	Frequency	50 Hz
TR2 parameters	Value	Pos. seq. resist. (Ohm)	0.1153

Vector group	YgD1	Zero seq. resist. (Ohm)	1.05e-3
Nominal power	12 MVA	Pos. seq. Inductance	0.413
Frequency	50 Hz	Zero seq. Inductance	3.32e-3
V1/V2 (KV)	120/25	Pos. seq. capacitance(F)	11.33e-9
Win. 1 Resistance	0.001 Pu	Zero seq. capacitance(F)	5-e9
Win. 1 Inductance	0.025 Pu	Line length (Km)	20
Win. 2 Resistance	0.001 Pu	Grid Parameters	Value
Win. 2 Inductance	0.025 Pu	Pos. seq. resist. (Ohm)	0.576
Mag. Resistance	500	Zero seq. Resist.	1.728
Mag. Inductance	Inf.	Pos. seq. Inductance	0.0183
		Zero seq. Inductance	0.055

Table A-3. PV parameters

PV parameters	Value	Converter Parameters	Value
Parallel strings	88	Number of bridge arms	3
Series module	7	Snubber resistance	1e6 ohm
Max. Power (W)	414.801	Power electronic device	IGBT/ Diodes
Cells per module	128	Internal resistance (Ron)	1e-3 ohm
V_{oc} (V)	85.3	IGBT forward volt.	0
I_{sc} (A)	60.9	Diode forward volt.	0
V_m (V)	72.9	Filter parameters	Value
I_m (A)	5.69	R (m ohm)	0.3745
α (%/deg.C)	-0.299	L (mH)	0.0994
β (%/deg.C)	0.03076	C (μ F)	0.1061

Table A-4. PV-Based Test System parameters

TR1 parameters	Value	TL Parameters/Km	Value
Vector group	YgD1	Frequency	60 Hz
Nominal power	25 MVA	Pos. seq. resist. (Ohm)	0.1153
Frequency	60 Hz	Zero seq. resist. (Ohm)	1.05e-3
V1/V2	25e3/250	Pos. seq. Inductance	0.413
Win. 1 Resistance	0.0012 Pu	Zero seq. Inductance (H)	3.32e-3
Win. 1 Inductance	0.03 Pu	Pos. seq. capacitance(F)	11.33e-9
Win. 2 Resistance	0.0012 Pu	Zero seq. capacitance(F)	5-e9
Win. 2 Inductance	0.03 Pu	Line length (Km)	14
Mag. Resistance	200	Grid Parameters	Value
Mag. Inductance	200	Pos. seq. resist. (Ohm)	0.576
TR2 parameters	Value	Zero seq. resist. (Ohm)	1.728
Vector group	YgD1	Pos. seq. Inductance	0.0183
Nominal power	47 MVA	Zero seq. Inductance	0.055
Frequency	60 Hz	Laod (2) parameters	Value
V1/V2 (KV)	120/25	V (KV)	25
Win. 1 Resistance	0.0027 Pu	F (HZ)	60

Win. 1 Inductance	0.08 Pu	P	30MW
Win. 2 Resistance	0.0027 Pu	QL	2MW
Win. 2 Inductance	0.08 Pu	QC	0
Mag. Resistance	500	Mag. Inductance	500